Saturation temperature effect on heat transfer coefficient during convective boiling in microfin tubes

L P M Colombo[1], A Lucchini[1], T N Phan[1], L Molinaroli[1], A Niro[1] and M Pozzoni[1]

[1]Dipartimento di Energia (Politecnico di Milano, via Lambruschini 4, 20156, Milano)
Corresponding author e-mail: luigi.colombo@polimi.it

Abstract. The growing attention on environmental aspects puts severe constraints on HVAC technology, mainly involving the working fluids and energy efficiency. Both are related to the main limiting factor of HVAC system: the heat transfer process, which, frequently, involves boiling and condensation. To provide suitable tools for the HVAC system design, it is necessary to gather information on the heat transfer characteristics of the new refrigerants. Particular interest is focused on R1234ze(e), because it is one of the viable options to face the R134a phase out. Something similar can be repeated for the low temperature ORC systems using a refrigerant as working fluid. Using a specifically designed test rig, heat transfer coefficient and pressure drop measures were performed during flow boiling of R1234ze(e). The operating conditions were defined by four parameters: the evaporation temperature (5 °C, 35 °C and 45 °C), the mass flux (two values were considered: 160 kg/m^{2}s and 220 kg/m^{2}s), the average thermodynamic quality (which varies between 0.25 and 0.75) and the quality change (which was fixed to 0.2). The uncertainty affecting the pressure drop and the heat transfer coefficient resulted lower than 1% and 5% respectively. The results highlighted that the saturation temperature strongly affects the heat transfer coefficient and the pressure drop: as a consequence of the saturation temperature increase from 5 °C to 45 °C, it was observed up to 40% heat transfer coefficient increase and 90% pressure drop reduction.

1. Introduction

Due to the increasing environmental concern the phase out of refrigerants commonly used in HVAC devices is taking place. It is very important to find suitable fluids for the tomorrow HVAC systems. The same can be said also for the low temperature ORC systems, which employ those refrigerants [1, 2]. One of the banned fluids is R134a and, among the new environmentally friendly fluids available, the hydro-fluoro-olefin (HFO) R1234yf and R1234ze(e) are possible replacements. They are characterized by a much smaller global warming potential and much shorter atmospheric lifetime than R134a. The manuscript aims to rate the performance of R1234ze(e) and reports the experimental investigation concerning the heat transfer coefficient and the pressure drop during flow boiling inside microfin tube J60. As a broad range of saturation temperatures can be met in HVAC and ORC common application, a sensitivity analysis, concerning its effect on the heat transfer process, is reported. Moreover, the experimental data are a very useful to benchmark the correlations, available in the open literature, to predict the pressure drop [3, 4, 5, 6, 7, 8, 9, 10] and the heat transfer coefficient [10, 11, 12, 13, 14, 15, 16, 17, 18]. Even though many researchers keep on working in this field, the topic proves to be very complex and a general purpose correlation, capable to properly describe the main effects related to boiling (the fluid properties and their dependence on the saturation temperature, the tube geometry, etc.), is still unavailable.

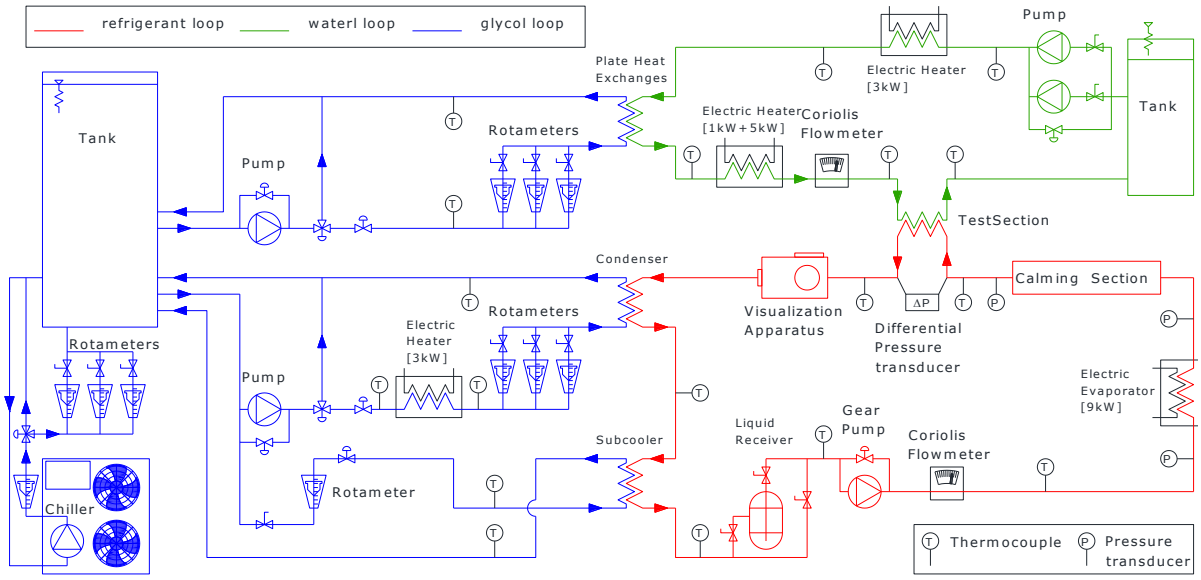

Figure 1. Main loops of the experimental apparatus.

2. Experimental apparatus

The experimental apparatus in Figure 1, is made of three main circuits named: the refrigerant loop (filled with R1234ze(e)), the water loop (filled with demineralized water) and glycol loop (filled with a mixture of water and ethylene glycol, 30 % volume concentration). They exchange thermal power each other in order to set the test condition and perform the experiments.

2.1. The glycol loop

The glycol loop, blue line in Figure 1, is a service circuit with two main tasks: to set the operating temperature in the test section, fixing the pressure in the condenser, and to chill both refrigerant and water. A commercial chiller (21 kW cooling capacity) cools the mixture to -10 °C and then it is stored in a 0.75 m^3 tank. Two independent loops, one for the water and the other for the refrigerant, are connected to the tank.

The loop dedicated to the water cools down the water entering in the test section, which heats up as a consequence of the viscous dissipation.

The other loop is in charge to set the temperature in the test section and to prevent cavitation in the pump. The former operation is accomplished setting the mass flow rate, using a manual needle valve, and the temperature (checked by a K-type thermocouple) at the condenser inlet, using a P.I.D. driven electric heater (nominal power 3 kW), such that the refrigerant pressure at the test section inlet (which is the sum of the pressure in the condenser and the pressure drop in between) be the saturation pressure corresponding to the test temperature. For the latter operation a bypass drains part of the cold mixture headed to the condenser to cool the liquid refrigerant entering the pump, the volume flow rate is tuned using a manual needle valve.

2.2. The water loop

The water loop, green line in Figure 1, is designed to exchange the thermal power required for the refrigerant phase change. The heat transfer takes place in a tube in tube heat exchanger (refrigerant in the inner duct, water in the annulus, the inner tube is made of copper while the outer tube is made of polymethyl methacrylate), named test section (Figure 2), thermally insulated from the surroundings with 100 mm thick shell of rubber foam. In the water loop there are two pumps of different size in parallel, according to the mass flow rate required, lower or higher than 300 kg/h, the smaller or the bigger is used. The pump drains the water from the tank (volume 0.2 m^3, thermally insulated with a rock-wool

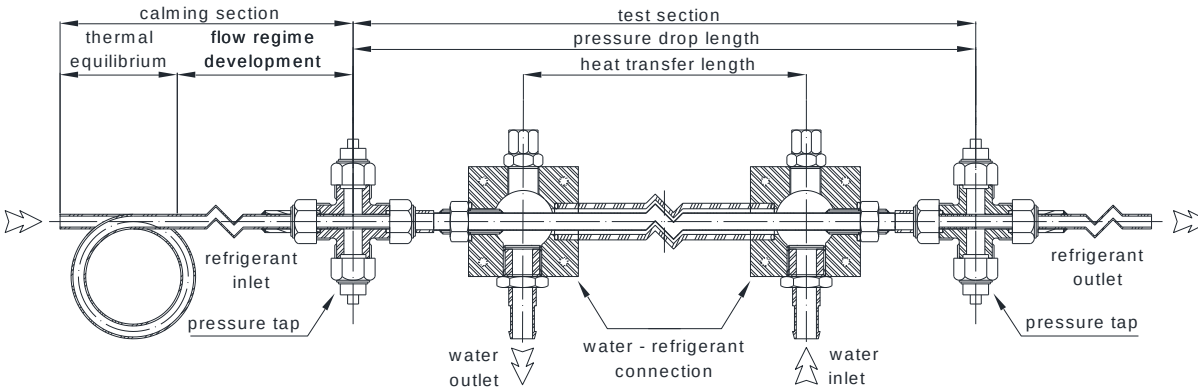

Figure 2. Test section main parts.

shell 5 cm thickness), a bypass and a manual needle valve fix the mass flow rate and its value is measured by a Coriolis flowmeter (range [0;400] kg/h, uncertainty 0.15 % of the reading). Afterwards a K-type thermocouple checks the water temperature and the flow enters in a plate heat exchanger, if cooling is required the glycol is flushed in the other side. Between the pump and the heat exchanger, as a safety device to prevent water freezing, there is a P.I.D. driven electric heater (nominal power 3 kW). After the plate heat exchanger, another P.I.D. driven electric heater (it is made of two elements: 1 kW and 5 kW, it is possible to use both or only one) sets the inlet temperature in the test section (checked by a K-type thermocouple) such that the power transfer reduces the water flow temperature of -2 °C (inlet and outlet temperature are provided by two groups of 3 K-type thermocouples connected in series, uncertainty 0.1 K). Finally the water returns to the tank.

2.3. The refrigerant loop

The main goal of the refrigerant loop, red line in Figure 1, is to provide, at the inlet of the test section, where the measures take place, a two phase flow of refrigerant at specified operating conditions, which are defined by the mass flow rate, the inlet quality and the inlet temperature.

A saturated liquid flow of refrigerant leaves the condenser (four plate heat exchanges and one shell end tube heat exchanger in parallel, depending on the thermal duty it is possible to use one or more of them) and enters in a plate heat exchanger (subcooler) to be chilled and to prevent cavitation in the circulation pump (gear type with inverter driven engine for the mass flow rate tuning). A Coriolis flowmeter (range [0;400] kg/h, uncertainty ±0.15 % of the reading) records the mass flow rate while a pressure transducer (relative, range [-1;30] bar, uncertainty ±1 % of full scale) and a thermocouple (K-type, uncertainty 0.1 K) check the thermodynamic state of the refrigerant as it enters in the evaporator (it is a set of 8 electric heaters, 9 kW total power, driven by a software control system) which provides the power to vaporize the amount of refrigerant specified by the test section inlet quality. A calming section, Figure 2, follows, it is made of two parts: a wrapped tube (outer diameter 9.52 mm, length 12 m, wrapping diameter 0.4 m, thermally insulated by a 5 cm thick rubber foam shell), which task is to get the thermal equilibrium between liquid and vapour of the two phase flow leaving the evaporator, and a straight duct (4.7 m long adiabatic duct and thermally insulated by a 5 cm thick rubber foam shell), designed for the development of the two phase flow regime. Then the refrigerant enters in the test section, pass by the visualization apparatus and, in the end, it returns to the condenser.

The test section, Figure 2, is a tube in tube heat exchanger (heat transfer length L=1.11 m) thermally insulated with 10 cm thick rubber foam shell. As different geometries are available for the inner surface of the refrigerant duct, the smooth tube is the reference. Their geometrical characteristics are reported in Table 1 while Figure 3 shows the differences.

A differential pressure transducer (range [-103.4;103.4] kPa, uncertainty ±0.1 % of the full scale), connected to two pressure taps separated by the distance L_p=1.3 m, records the pressure drop. While a relative pressure transducer (range [-100;1600] kPa, uncertainty ±0.25 % of the full scale), connected to the tap at the inlet of the test section, reads the refrigerant pressure. The refrigerant inlet and outlet

Table 1. Microfin tube geometrical characteristics.

Parameter			**J60**	**smooth**
inner diameter (fin root)	D_r	[mm]	8.96	8.92
outer diameter	D	[mm]	9.52	9.52
wet perimeter	S_p	[mm]	44.9	28.0
cross section area	A_c	[mm^2]	62.2	62.5
hydraulic diameter	D_h	[mm]	5.28	8.92
exchanging area ratio			1.68	1
fin number	n	[-]	60	
height	H	[mm]	0.2	
apex angle	α	[°]	40	
helix angle	β	[°]	18	

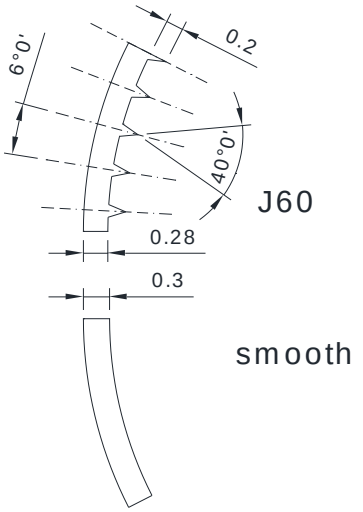

Figure 3. Microfin tube geometry.

temperatures are the saturation temperatures given by the pressure readings. Two groups (one at the entrance and one at the exit) of three thermocouples are glued inside grooves (length 50 mm, depth 0.15 mm, width 0.4 mm) on the outside of the inner tube (top, side and bottom position), to measure the wall temperatures, further details are reported in [19]. The reference junction of each thermocouple (K-type, uncertainty 0.1 K) is inserted in a Dewar flask filled with melting ice.

3. Data reduction

Preliminary tests, involving a test section built using a smooth and single phase flow of refrigerant, highlighted the right functioning of the facility, as:

- the power transferred computed for both the refrigerant side and the water side matched within ±5%;
- there is agreement within ±5 % with the most commonly used correlations for heat transfer and pressure drop.

The experimental activity is made of two main parts: the data recording and post processing (their complete description is reported in [19]). During the former a computer stores the reading of the measuring devices and, as it ends, the latter provides:

- the experimental conditions, namely the main quantities related to the refrigerant flow in the test section: the inlet saturation temperature T_{ri}, the mass flux G, the quality change Δx, the average quality x_m;
- the pressure drop per unit length $\Delta p/L_p$;
- the heat transfer coefficient h.

The data recording takes place when the system is in steady state, each acquisition runs for 180 s with a sampling frequency of 1 Hz and store 181 readings for every quantity. For each experimental condition 12 acquisitions are repeated. The data of a single acquisition are the averages of the 181 readings and, in a similar fashion, the data corresponding to a single experimental condition are the mean values of the 12 acquisitions.

The post processing begins computing the refrigerant inlet temperature in the test section, which is the saturation temperature corresponding to the inlet pressure:

$$T_{\mathrm{ri}} = T_{\mathrm{sat}}(p_{\mathrm{ri}}) \tag{1}$$

The same procedure is used for the outlet temperature:

$$T_{\mathrm{ro}} = T_{\mathrm{sat}}(p_{\mathrm{ri}} - \Delta p) \tag{2}$$

Referring to the nominal geometrical features of the microfin tube, the net cross section area is:

$$A_{\mathrm{c}} = \frac{\pi D_{\mathrm{r}}^2}{4} - \frac{nH^2}{\cos\beta}\tan\left(\frac{\alpha}{2}\right) \tag{3}$$

From the Coriolis flowmeter reading, the refrigerant mass flux is computed as follows:

Table 2. R1234ze(e) thermal properties, part (a) reports the numerical values of density, dynamic viscosity, thermal conductivity and phase change enthalpy while part (b) reports the percentage variation of the afore mentioned quantities compared to T_{sat}=5 °C.

Numerical values (a)

T_{sat}	[°C]	5		35		45	
phase		L	V	L	V	L	V
ρ	[kg·m^{-3}]	$1.22\cdot10^{3}$	$1.39\cdot10^{1}$	$1.13\cdot10^{3}$	$3.53\cdot10^{1}$	$1.09\cdot10^{3}$	$4.67\cdot10^{1}$
μ	[kg·m^{-1}·s^{-1}]	$2.46\cdot10^{-4}$	$1.10\cdot10^{-5}$	$1.68\cdot10^{-4}$	$1.28\cdot10^{-5}$	$1.48\cdot10^{-4}$	$1.35\cdot10^{-5}$
k	[W·m^{-1}·K^{-1}]	$8.14\cdot10^{-2}$	$1.19\cdot10^{-2}$	$7.09\cdot10^{-2}$	$1.45\cdot10^{-2}$	$6.77\cdot10^{-2}$	$1.55\cdot10^{-2}$
h_{lv}	[kJ·kg^{-1}]	181		159		150	

Percentage variation (b)

T_{sat}	[°C]	35		45	
phase		L	V	L	V
$V_{ρ\%}$	[-]	-8%	154%	-11%	236%
$V_{μ\%}$	[-]	-32%	17%	-40%	22%
$V_{k\%}$	[-]	-13%	22%	-17%	30%
$V_{hlv\%}$	[-]	-12%		-17%	

$$G = \frac{\dot{m}_\mathrm{r}}{A_\mathrm{c}} \tag{4}$$

Assuming negligible the thermal dispersion in the test section, power transfer takes place only between water and refrigerant:

$$\dot{Q} = \dot{m}_\mathrm{a} c_\mathrm{pa} (T_\mathrm{ai} - T_\mathrm{ao}) \tag{5}$$

The quality change can be computed as:

$$\Delta x = (x_\mathrm{o} - x_\mathrm{i}) = \frac{\dot{Q}}{\dot{m}_\mathrm{r} h_\mathrm{lv}(p_\mathrm{ri})} \tag{6}$$

Focusing on the evaporator and assuming negligible thermal dispersion, the energy balance provides the inlet quality:

$$x_\mathrm{i} = \frac{\dot{Q}_\mathrm{e} - \dot{m}_\mathrm{r} c_\mathrm{pr} [T_\mathrm{sat}(p_\mathrm{r}) - T_\mathrm{re}]}{\dot{m}_\mathrm{r} h_\mathrm{lv}(p_\mathrm{ri})} \tag{7}$$

In the end the mean quality in the test section is:

$$x_\mathrm{m} = x_\mathrm{i} + \frac{\Delta x}{2} \tag{8}$$

The pressure drop per unit length is immediately computed because the total pressure drop Δp is given by the differential pressure transducer and the distance L_p between the pressure tabs, which is a design parameter, was checked at the end of the building process.

The procedure to compute the average heat transfer coefficient h in the test section is based on the logarithmic mean temperature between the wall and the refrigerant. The wall temperature is determined averaging the readings of three thermocouples placed on the outside of the microfin tube and located in the same cross-section.

$$T_\mathrm{w} = \frac{T_\mathrm{t} + T_\mathrm{s} + T_\mathrm{b}}{3} \tag{9}$$

It follows that the logarithmic mean temperature difference is:

$$\Delta T_\mathrm{ml} = \frac{(T_\mathrm{wo} - T_\mathrm{ro}) - (T_\mathrm{wi} - T_\mathrm{ri})}{\ln \frac{T_\mathrm{wo} - T_\mathrm{ro}}{T_\mathrm{wi} - T_\mathrm{ri}}} \tag{10}$$

The heat transfer area of the refrigerant duct refers to the fin root diameter, hence the heat flux is:

$$q = \frac{Q}{\pi D_\mathrm{i} L} \tag{11}$$

Finally, the average heat transfer coefficient is given by the following equation:

$$h = \frac{q}{\Delta T_\mathrm{ml}} \tag{12}$$

The propagation uncertainty analysis (further details can be found in [19]) showed that, for each data-point, the uncertainty related to the parameters identifying the operating conditions, the pressure drop per unit length and the heat transfer coefficient is lower than 5 %.

4. Experimental results

The experiments focused on R1234ze(e) during flow boiling and mainly aimed to check the saturation temperature effect on the heat transfer performances. They were performed tuning the mean quality in the range $x_m \in [0.25;0.75]$, three inlet saturation temperatures were tested (T_{ri}=5 °C, which was chosen a reference in the comparisons, T_{ri}=35 °C and T_{ri}=45 °C), two mass fluxes were taken into account (G=163 kg/m^{2}s and G=220 kg/m^{2}s) and the quality change was fixed (Δx=0.2) while the heat flux (referred to the fin root diameter) is in the range $q \in [10;17]$ kW/m^2, because the phase change enthalpy is a decreasing function of the saturation temperature. About the selection of the temperatures it has to be highlighted that: the reference temperature (T_{ri}=5 °C) is the standard evaporating temperature for HVAC systems, while, the others represent a compromise between the lower evaporation temperatures in ORC systems (55 ÷ 65 °C) [1] and the upper limit of the experimental facility to prevent the damaging of the test section, which has parts made of polymethyl methacrylate (softening temperature 60÷70°C).

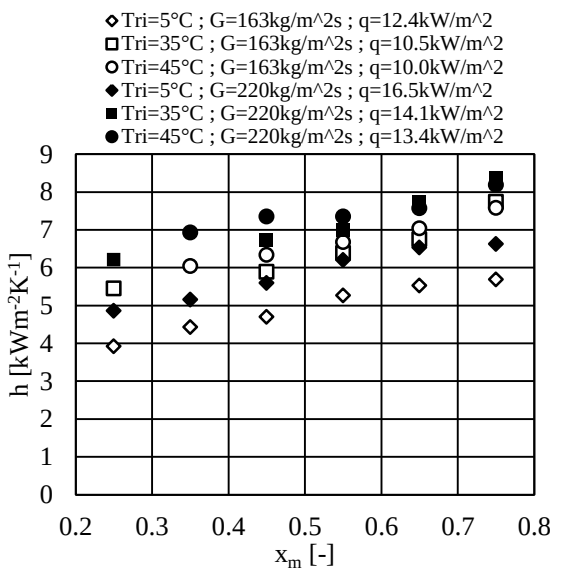

Figure 4. Heat transfer coefficient versus mean quality (quality change Δx=0.2).

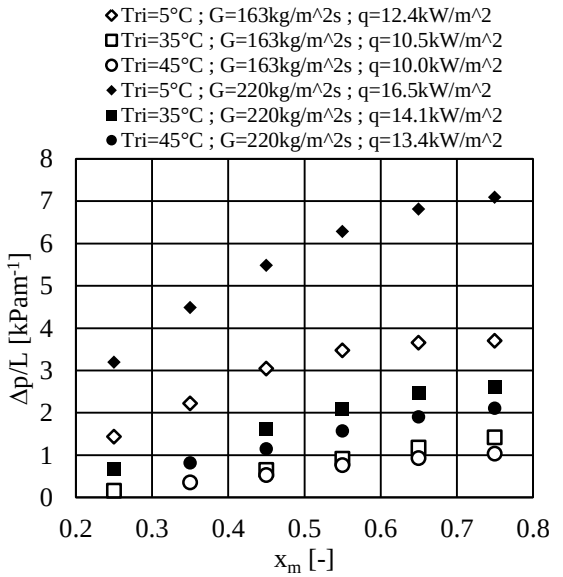

Figure 5. Pressure drop per unit length versus mean quality (quality change Δx=0.2).

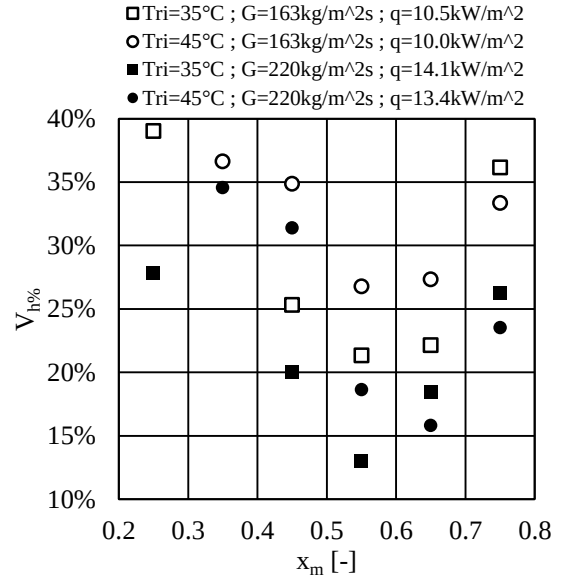

Figure 6. Heat transfer coefficient percentage variation versus mean quality (quality change: Δx=0.2, reference temperature: T_{sat}=5 °C).

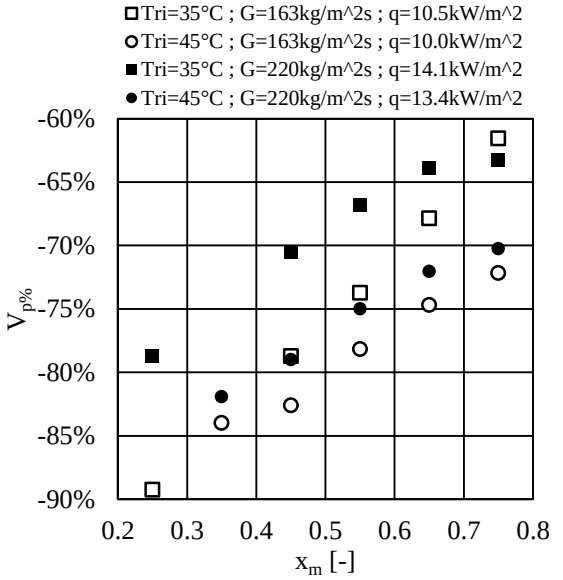

Figure 7. Pressure drop per unit length percentage variation versus mean quality (quality change: Δx=0.2, reference temperature: T_{sat}=5 °C).

Table 2 sums up the main R1234ze(e) thermal properties (part a) at different operating conditions and their percentage variation (part b), compared to the reference, which are computed according to the following equation (where Z is a generic quantity):

$$V_{z\%} = \frac{Z}{Z_R} - 1 \tag{13}$$

As already observed in previous works (for instance [19]), the heat transfer coefficient (figure 4) and the pressure drop per unit length (figure 5) grow as the mass flux increases.
The effect of the saturation temperature on the heat transfer coefficient and the pressure drop per unit length can be understood checking their percentage variations, which are depicted in figure 6 and figure 7 respectively. To properly perform the analysis some remarks concerning table 2 part (b) are required:

A. the phase change enthalpy decreases as the saturation temperature increase;
B. the vapour thermal conductivity increases as the saturation temperature increase;
C. the liquid thermal conductivity decreases as the saturation temperature increase;
D. the vapour thermal conductivity increase is almost twice the liquid thermal conductivity reduction;
E. the liquid thermal conductivity and the phase change enthalpy reduce almost of the same amount;
F. the liquid dynamic viscosity largely reduces as the saturation temperature increases;
G. the largest effect of temperature change is on the vapour density.

According to figure 4 the heat transfer coefficient increases as the saturation temperature grows, while the heat flux, as a consequence of remark A, reduces in order to keep Δx constant, while figure 6 shows that the percentage increase of the heat transfer coefficient is in the range $V_{h\%} \in [10\ \% ; 40\ \%]$ and its trend is not monotonic. From equation 12, it follows that the logarithmic mean temperature should reduce more than the heat flux does as the saturation temperature rises. Figure 6 reveals that the heat transfer coefficient variation depends on the mean quality and it has a minimum in the range $x_m \in [0.25;0.75]$. It seems to suggest that the flow regime has an influence on it. A possible explanation of the trend in figure 6 could be the following:

- $\mathbf{x_m < 0.3}$: as intermittent flow could be expected a significant portion of the tube wall is in touch with the vapour, according to remark B, as the saturation temperature rises, the wall temperature should be closer to the fluid temperature and a larger heat transfer coefficient could be expected as the saturation temperature increases;
- $\mathbf{x_m \geq 0.3}$: as annular flow should be present the tube wall is adjoined only by the liquid while the vapour is in the core of the flow. According to remark E, the temperature gradient in the liquid

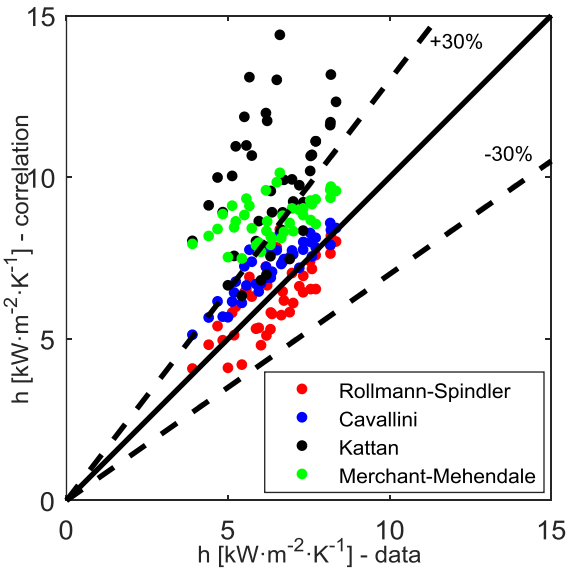

Figure 8. Heat transfer coefficient: data versus predictions for some correlations.

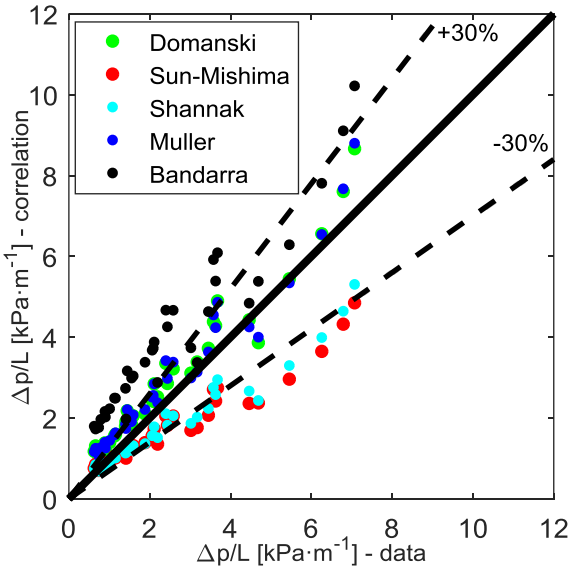

Figure 9. Pressure drop per unit length: data versus predictions for some correlations.

Table 3. Comparison between data (the reference value) and correlations, the mean percentage variation and the standard deviation for the heat transfer coefficient are in part (a) while part (b) reports their values for the pressure drop per unit length.

Heat transfer coefficient (a)			**Pressure drop per unit length (b)**		
correlation	$V_{h\%m}=\Sigma_i V_{h\%i}/N$	$\sigma_{\%}$	**correlation**	$V_{p\%m}=\Sigma_i V_{p\%i}/N$	$\sigma_{\%}$
Cavallini	13.2%	10.0%	**Bandarra**	72.2%	44.1%
Han	-35.7%	14.4%	**Domanski**	24.9%	21.9%
Kattan	56.7%	35.0%	**Goto**	-20.6%	21.2%
Merchant	38.8%	23.1%	**Kuo-Wang**	33.8%	23.9%
Murata	-25.6%	27.4%	**Müller-Steinhagen**	25.5%	21.8%
Rollmann	-2.3%	12.9%	**Shannak**	-21.9%	14.8%
Yun	-79.1%	8.1%	**Sun-Mishima**	-23.8%	17.1%

film should be approximately independent of the saturation temperature while the temperature gradient in the vapour core, because of remark B, should reduce as the saturation temperature increases. As suggested by remark D and E the logarithmic mean temperature should reduce more than the heat flux and lead to a larger heat transfer coefficient. The minimum is in the range $x_m \in [0.55;0.65]$ where liquid layer thickness becomes almost uniform, as the thickness reduces the heat transfer variation rises again.

The pressured drop per unit length reduces as the saturation temperature grows (figure 5), that could be the consequence of two combined effect listed in remarks F and G (which implies a significant reduction of the mean flow velocity as the saturation temperature rises). The reduction is in the range $V_{p\%} \in$ [-90 %;-60 %] and reduces as the mean quality grows (figure 7).

5. Correlations

The comparison between the data and the correlations prediction was performed drawing the parity plots (to make them readable some correlations were not included) for the heat transfer coefficient, in figure 8, and the pressure drop per unit length in figure 9. Moreover, the mean percentage variation $V_{\%m}$ and the standard deviation σ were used to deem the predictive capability of the correlations. Table 3 reports their values for the heat transfer coefficient, part (a), and the pressure drop per unit length, part (b).

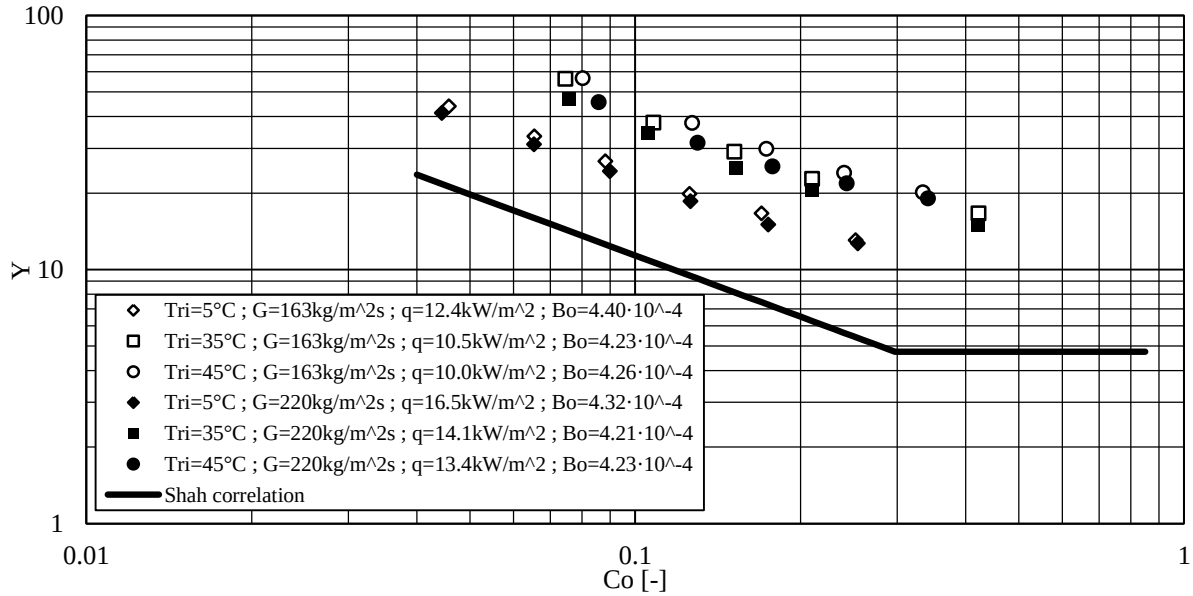

Figure 10. Comparison between the heat transfer data and the Shah model.

According to table 3 and figure 8 Rollman and Cavallini correlations properly account for the saturation temperature effect and provide the best predictions for the heat transfer coefficient.
Figure 10 shows the heat transfer data and the Shah model [17, 18], which was not included in table 3 because it was developed for the smooth tube and, as expected, it is unable to properly predict the data, nevertheless, it correctly gets their trend and highlights the temperature influence hiding the mass flux effect. About pressure drop per unit length, table 3 part (b) and figure 9 suggests that all the correlations, but the one proposed by Bandarra, provide acceptable predictions and have very similar performances (Shannak's correlation seems to be the best).

6. Conclusions

The experiments highlighted that the heat transfer coefficient is an increasing function of the saturation temperature while the pressure drop per unit length is a decreasing function. The percentage variation of the heat transfer coefficient seems to be affected by the flow regime, the smallest values seems to be recorded for the fully developed annular flow. The comparison between the experimental data and the predictions shows that all the correlations for pressure drop reported in the manuscript, but two cases, provide a good agreement. On the contrary only the Rollmann and Cavallini correlations can take into account properly the saturation temperature effect.

7. Acknowledgments

The financial support of MIUR through the program PRIN 2015 (Grant Number 2015M8S2PA) is greatly acknowledged.

Nomenclature

Latin symbols

A_c	cross section area [m^{-2}]	Q_e	power provided by the evaporator [W]
Co	convection number [-]	S_p	wet perimeter [m]
c_{pa}	water specific heat capacity [$J \cdot kg^{-1} \cdot K^{-1}$]	T_{ai}	water inlet temperature [K]
c_{pr}	refrigerant specific heat capacity [$J \cdot kg^{-1} \cdot K^{-1}$]	T_{ao}	water outlet temperature [K]
D	outer diameter [m]	T_b	temperature in the bottom position [K]
D_h	hydraulic diameter [m]	T_{ri}	refrigerant temperature, test section inlet [K]
D_r	inner diameter (fin root) [m]	T_{re}	refrigerant temperature, evaporator inlet[K]
G	refrigerant mass flux [$kg \cdot m^{-2} \cdot s^{-1}$]	T_{ro}	refrigerant temperature, test section outlet [K]
H	fin height [m]	T_s	temperature in the side position [K]
h	heat transfer coefficient [$W \cdot m^{-2} \cdot K$]	T_{sat}	saturation temperature [K]
h_{lv}	liquid vapour phase change enthalpy [$J \cdot kg^{-1}$]	T_t	temperature in the top position [K]
k	thermal conductivity [$W \cdot m^{-1} \cdot K^{-1}$]	T_{wi}	mean wall temperature, refrigerant inlet [K]
L	heat transfer length [m]	T_{wo}	mean wall temperature, refrigerant outlet [K]
L_p	distance between the pressure taps [m]	$V_{z\%}$	percentage variation of quantity Z [-]
$\dot{m}_a$	water mass flow rate [$kg \cdot s^{-1}$]	x_i	refrigerant inlet quality [-]
$\dot{m}_r$	refrigerant mass flow rate [$kg \cdot s^{-1}$]	x_m	mean quality in the test section [-]
n	fin number [-]	x_o	refrigerant outlet quality [-]
p_{ri}	refrigerant inlet pressure [Pa]	Y	enhancement factor [-]
Q	power exchanged in the test section [W]	Z	generic quantity [-]
q	heat flux [$W \cdot m^{-2}$]	Z_R	generic quantity, at the reference condition [-]

Greek symbols

α	apex amgle [°]	Δx	quality change [-]
β	helix angle [°]	μ	dynamic viscosity [kg·m-1·s-1]
Δp	pressure drop [Pa]	ρ	density [kg·m-3]
ΔT_{ml}	log mean temperature difference [K]		

References

[1] Molés F, Navarro-Esbrí J, Peris B, Mota-Babiloni A, Mateu-Royo C 2017 *Energy Procedia* **142** 1192-98
[2] Longo G A, Mancin S, Righetti G, Zilio C, Brownb J S 2020 Applied Thermal Engineering **167**

[3] Choi Y J, Kedzierski A M and Domanski A P 2001 *Proceedings of IIF-IIR Commission B1*. Paderborn, Germany, **B4** 9–16
[4] Shannak B A 2008 *Nuclear Engineering and Design* **238(12)** 3277–84
[5] Sun L and Mishima K 2009 *International Journal of Multiphase Flow* **35(1)** 47–54
[6] Bandarra Filho E P, Saiz Jabardo J M and EL Barbieri P 2004 *International journal of refrigeration* **27(8)** 895–903
[7] Muller-Steinhagen H and Heck K 1986 *Chemical Engineering and Processing: Process Intensification* **20(6)** 297–308
[8] Goto M, Inoue N and Ishiwatari N 2001 *International Journal of Refrigeration*, **24** 628–638
[9] Kuo C S and Wang C C 1996 *International Journal Heat Mass Transfer*, **39** 2559–69
[10] Rollmann P and Spindler K 2016 *International Journal of Thermal Sciences* **103** 57-66
[11] Cavallini A, Del Col D, Doretti L, Longo G A and Rossetto L 1999 *Heat and Technology* **17(2)** 29–36
[12] Kattan N, Thome J R, and Favrat D 1997 *Convective Flow and Pool Boiling Conference*. Irsee, Germany, May 18th-23rd
[13] Merchant R and Mehendale S 2016 *Proceedings of the ASME International Mechanical Engineering Congress and Exposition*. Phoenix, Arizona, November 11th-17th
[14] Han X H, Fang Y B, Wu M, Qiao X G and Chen G M 2017 *International Journal of Heat and Mass Transfer* **104** 276–287
[15] Yun R, Kim Y, Seo K and Kim Y 2001 *International Journal of Heat and Mass Transfer* **45** 2003-10
[16] Murata K and Hashizume K 1993 *Journal of Heat Transfer* **115** 680–689.
[17] Shah M M 1976 *ASHRAE Transaction* **82(2)** 66-86
[18] Shah M M 1982 *ASHRAE Transaction* **88(1)** 185-196
[19] Colombo L P M, Lucchini A, Phan T N, Molinaroli L and Niro A. 2019 *Journal of Physics: Conf. Series* **1224** 012037